https://doi.org/10.17816/OV15931

FOCAL OSSIFICATION AS ONE OF THE REASONS FOR ERRONEOUS DIAGNOSIS OF CHORIORETINAL LESIONS

© *A.S. Stoyukhina*

Research Institute of Eye Diseases, Moscow, Russia

For citation: Stoyukhina AS. Focal ossification as one of the reasons for erroneous diagnosis of chorioretinal lesions. *Ophthalmology Journal*. 2019;12(3):31-39. https://doi.org/10.17816/OV15931

Received: 02.08.2019 Revised: 20.08.2019 Accepted: 19.09.2019

✧ Focal calcifications of the retina and choroid occur usually in such well-known tumors as: retinoblastoma, choroidal osteoma, choroidal hemangioma, retinal astrocytoma. In addition, cases of idiopathic or secondary calcification are known, the most common of them is sclerochoroidal calcification. The article provides a detailed analysis of the clinical and tomographic pictures of ossifying conditions occurring in adults. It is shown that, in addition to a different ophthalmoscopic picture, these conditions are characterized by a different level of localization of the pathological calcification zone and a different stage of retinal damage.

✧ ***Keywords:*** sclerochoroidal calcification; choroidal osteoma; retinal astrocytoma; optical coherence tomography.

ЛОКАЛЬНОЕ ОБЫЗВЕСТВЛЕНИЕ КАК ОДНА ИЗ ПРИЧИН ОШИБОЧНЫХ ДИАГНОЗОВ ХОРИОРЕТИНАЛЬНОГО ПОРАЖЕНИЯ

© *А.С. Стоюхина*

ФГБНУ «НИИ глазных болезней», Москва

Для цитирования: Стоюхина А.С. Локальное обызвествление как одна из причин ошибочных диагнозов хориоретинального поражения // Офтальмологические ведомости. – 2019. – Т. 12. – № 3. – С. 31–39. https://doi.org/10.17816/OV15931

Поступила: 02.08.2019 Одобрена: 20.08.2019 Принята: 19.09.2019

✧ Локальные обызвествления сетчатки и хориоидеи встречаются, как правило, при таких известных опухолях, как ретинобластома, остеома хориоидеи, гемангиома хориоидеи, астроцитома сетчатки. Наряду с этим известны случаи обызвествления, имеющие идиопатический или вторичный характер, наиболее распространена из них склерохориоидальная кальцификация. В статье приведён подробный анализ клинической и томографической картины оссифицирующих состояний, встречающихся во взрослом возрасте. Показано, что помимо различной офтальмоскопической картины данные состояния характеризуются разным уровнем локализации зоны патологического обызвествления и разной степенью поражения сетчатки.

✧ ***Ключевые слова:*** склерохориоидальная кальцификация; остеома хориоидеи; астроцитома сетчатки; оптическая когерентная томография.

Local calcifications of the retina and choroid usually occur in well-known tumors such as retinoblastoma (RB), choroidal osteoma (CO), choroidal hemangioma (CH), and retinal astrocytoma (RA). In addition, cases of idiopathic or secondary calcification are known; the most common case among them is sclerochoroidal calcification (SCC).

These diseases should be differentiated primarily from melanoma and metastatic lesions of the choroid [1–3]. However, in clinical practice, these potential changes are often perceived as the outcome of inflammatory processes in the chorioretinal complex, which can lead to inadequate management of the patient.

Nonetheless, CO, sclerochoroidal calcification, and RA represent the greatest diagnostic difficulties. Unfortunately, in these clinical situations, ultrasound examination (US), which is the "gold standard" for the diagnosis of intraocular neoplasms, yields little information. Clinical observations on the echograms typically exhibit CO, SCC, and RA as extended hyperreflective foci in the chorioretinal complex

zone creating the acoustic shadow phenomenon [4–7], whereas CH and RB are characterized by the formation of point hyperechoic inclusions in the tumor tissue [7–9].

Choroidal osteoma (ossifying choristoma) is a rare benign tumor characterized by the formation of mature bone tissue in the choroid [10, 11]. It is detected mainly in women in their second or third decades of life [4, 5], although current literature has presented cases of CO in a 4-month premature newborn [12] and in a 68-year-old patient [13].

The CO growth is inactive; hence, visual disturbances tend to develop very slowly. In 31%–47% of cases, osteoma leads to decreased vision due to the formation of a subretinal neovascular membrane (SNM) [2, 5, 14].

A morphological study on the choriocapillaries layer and the outer layers of the choroid revealed a bone tissue of a cellular type, represented by bone trabeculae penetrated by dilated thin-walled vessels [10, 11].

Furthermore, CO is ophthalmoscopically localized in the macular or juxtapapillary zone and it is primarily identified by its single yellowish or orange node with clear boundaries and an uneven surface [4, 5, 14, 15]. A network of its own vessels is usually revealed on the node surface [2, 5] and the lesion is unilateral in 66%–80% cases [5, 15]. However, and during the follow-up, current literature has pinpointed the CO development in the fellow eye [16] or the appearance of a second focus on the affected eye [17].

Ultrasound examinations have validated the possibility of spontaneous decalcification of CO during the follow-up period, as well as following treatment outcomes (laser coagulation, photodynamic therapy) [2, 4, 5], which leads to the development of retinal pigment epithelium (RPE) and choriocapillaries atrophy [4, 5]. According to optical coherence tomography (OCT), it was proved that SNM, which leads to a decrease in vision, develops at the border of calcified and decalcified sites [2, 14]. The RPE rupture, occurring sometimes following intravitreal administration of anti-VEGF drugs used to treat SNM, can also lead to a marked decrease in vision [18].

Sclerochoroidal calcification is a rare benign calcification of the choroid and sclera. In most cases (79%), the process is idiopathic, and SCC can also occur along with hereditary renal tubular diseases (such as Bartter and Gitelman syndromes), chronic renal failure, Albright's hereditary osteodystrophy, along with conditions that lead to hypercalcemia and hypomagnesemia, such as hyperparathyroidism, pseudohypoparathyroidism, intoxication with vitamin D, sarcoidosis, or hypophosphatemia [19–22]. SCC is most often detected in Caucasian women aged 47–88 years [19, 21, 23]. The process is bilateral in almost half cases, [19, 23, 24]. However, a multifocal lesion is also possible [23]. Vision prognosis is favorable even with the multifocal form of SCC because the foveolar zone remains intact [19, 25], a fact that can be explained by the predominant localization of the process along the supero-temporal vascular arcade. This is associated with the constant influence of force at the superior oblique muscle site of attachment [19, 20]. Moreover, SCC is ophthalmoscopically represented by a yellowish, slightly protruding lesion with a crescent shape and with clear boundaries, an uneven surface and areas of RPE atrophy on the surface.

Retinal astrocytic hamartoma (astrocytoma) is a benign glial tumor that tends to develop from retinal nerve fibers layer. It is primarily revealed by accident in young patients, and both sporadic (29%) and syndrome-associated cases of RA have been previously described [26]. In the syndrome-associated form, RA is most often one of the manifestations of tuberous sclerosis [26–28]. Furthermore, retinal astrocytic hamartoma can be combined with pigmented retinitis, neurofibromatosis, or myelinic fibers [26, 27]. RA is usually asymptomatic; however, the development of secondary exudative retinal detachment, including isolated detachment in the macular zone, can lead to the manifestation of hemophthalmia, or neovascular glaucoma, visual impairment [27, 28].

Astrocytoma is primarily localized in the fundal central zone. Two forms of this formation, the non-calcified and calcified ones, have been previously described [1, 28], and a combined version of the two forms is also possible [28].

Calcified astrocytoma is ophthalmoscopically represented by a delimited node of white or yellow–white color, which can become mulberry-shaped because of the development of surface cysts [9, 28]. Biomicrophthalmoscopy examinations have revealed that this condition is associated with point zones of calcification of intense white color [9].

In most cases, the correct diagnosis of local chorioretinal calcifications can be performed based on a detailed analysis of the ophthalmoscopic picture. However, in certain complicated cases, OCT of the retina can provide significant diagnostic assistance. Nevertheless, current research has merely provided

a detailed description of specific individual cases. Attempts have been made to group the respective OCT signs from various tumors of the choroid and retina in order to facilitate their clinical differentiation [29]. However, literature fails to provide any analysis pertaining to these differential signs facilitating the establishment of a correct diagnosis of the retina and choroid local calcifications, and thus provide an efficient therapeutic approach.

Therefore, this work aimed to analyze results stemming from OCT studies in patients with CO, SCC, and RA.

MATERIALS AND METHODS

10 patients were examined (5 with SCC, 3 with CO, and 2 with RA).

Ophthalmoscopy examinations were performed according to the established procedure, and OCT was implemented in both the standard and in the EDI (enhanced depth imaging) mode (OCT Spectralis, Heidelberg Engineering, Germany). Consequently, tomograms were analyzed in shades of gray, whereas the foci diameters were measured on infrared images of the fundus obtained by OCT.

Furthermore, we used the commercially available IBM SPSS Statistics 23.0 software to perform the statistical analysis of the acquired results.

RESULTS AND DISCUSSION

The age of SCC patients (5 patients, 6 eyes) ranged from 59 to 73 years (mean age was 68.0 ± 2.78 years). In the case of bilateral multifocal lesion (1 patient) (Fig. 1), the presence of "atrophic" foci in the middle periphery of both eyes was noted in the medical documentation from a different clinic. Ultrasound examinations revealed this feature as extended hyperechoic areas concurrent with an acoustic shadow that was regarded as the outcome of chorioretinitis. On the other hand, the foci were revealed accidentally in the remaining cases (4 patients, 4 eyes).

The maximum corrected visual acuity (MCVA) on the affected eye was almost identical to the fellow eye (average was 0.73 ± 0.17 and 0.83 ± 0.09, respectively) ($p = 0.28$). In one case, a MCVA decrease of 0.07 to the affected eye was caused by the presence of concomitant stage IV glaucoma. In other cases, a 0.8 decrease in vision was caused by age-related lens alterations.

The foci were usually located at a distance of 3.22 ± 0.39 mm from the foveola, they had clear boundaries and a white–yellow pigmentation along the margins. Furthermore, these foci exhibited areas of pigment accumulation, and ophthalmoscopic signs of retinal atrophy were found in the central part of the foci. Most often, the foci had an oval (5 lesions) or a crescent shape (four lesions), with almost equal diameters (5.66 ± 0.54 and 5.98 ± 0.57 mm, respectively). In the multifocal lesion, one focus exhibited a round shape (2.3 mm in diameter) and two foci exhibited an irregular shape, in which the maximum diameters were 11.5 and 12.5 mm, respectively. This suggests that the focus shape indicates the duration of the process.

In cases of single-focus lesions (4 eyes), the foci were located along the supero-temporal arcade.

Three years after the initial visit, one patient presented a second focus that was revealed on the

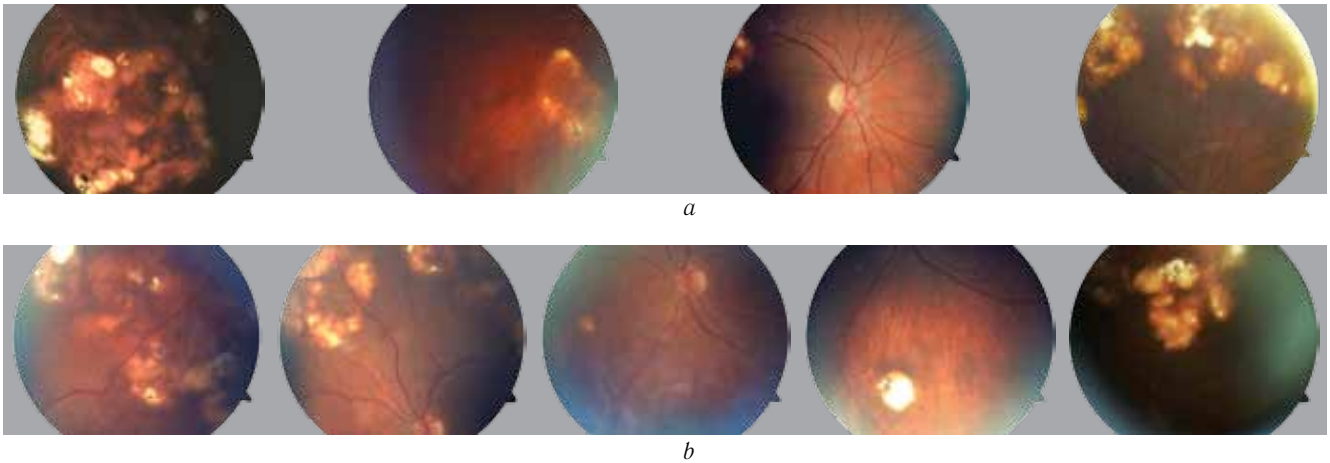

a

b

Fig. 1. Right (*a*) and left (*b*) eye fundus photo of patient B., 72 years old, with bilateral multifocal sclerochoroidal calcification

Рис. 1. Фото глазного дна правого (*a*) и левого (*b*) глаза пациентки Б., 72 года, с билатеральной многофокусной склерохориоидальной кальцификацией

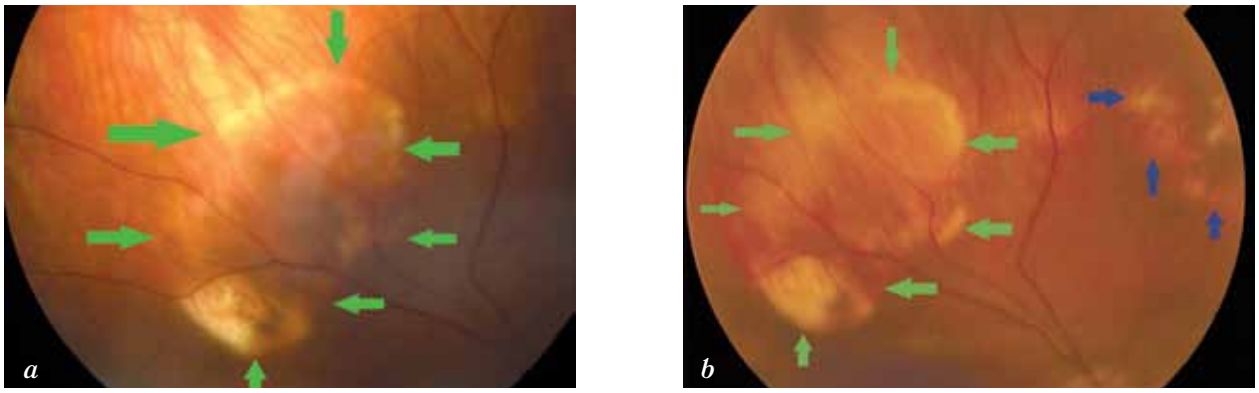

Fig. 2. Fundus photo of patient Sh., 59 years old at first visit, and after 38 months follow-up (green arrows – borders of the first focus, blue arrows – borders of the second focus)

Рис. 2. Фото глазного дна пациентки Ш., 59 лет: при первом осмотре (*a*) и через 38 мес. (*b*) (границы первого очага — зелёные стрелки, границы второго очага — синие стрелки)

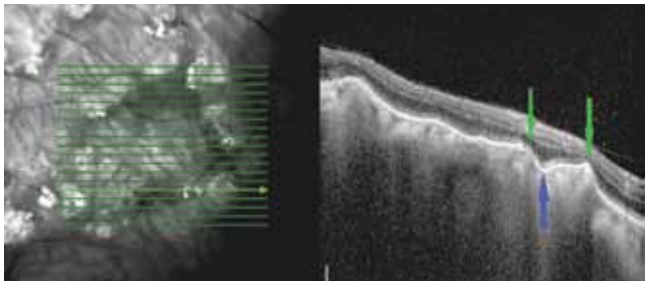

Fig. 3. Optical coherence tomography of the patient B. (72 years old). Horizontal scan across sclerochoroidal calcification. Green arrows – "spiky" Bruch's membrane profile, blue arrows – Bruch's membrane "entrapment" area

Рис. 3. Оптическая когерентная томография пациентки Б., 72 года. Горизонтальный срез через зону склерохориоидальной кальцификации. Зелёные стрелки — «пикообразный» профиль мембраны Бруха; синяя стрелка — зона «западения» мембраны Бруха

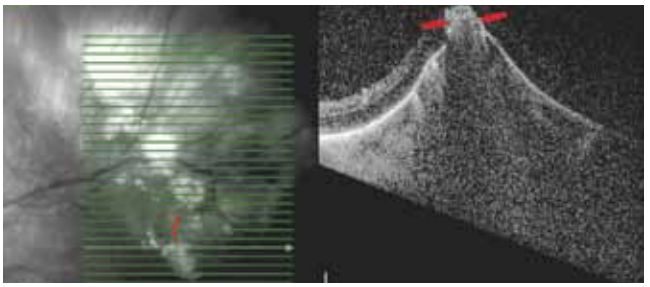

Fig. 4. Optical coherence tomography of the patient T. (64 years old). Horizontal scan across sclerochoroidal calcification. Arrows – area of retinal damage, visualization of the outer border of the underlying choroid is impaired

Рис. 4. Оптическая когерентная томография пациента Т., 64 года. Горизонтальный срез через нижнюю часть очага. Стрелки — зона повреждения сетчатки, нарушена визуализации наружной границы подлежащей хориоидеи

fundus (Fig. 2). It should be noted that additional calcifications in the Achilles tendon of this patient were simultaneously revealed.

Three female patients aged 59, 72, and 73 years, respectively, had indications of a systematic process in history, namely changes in the biochemical analysis of their blood indicating a mineral metabolism disorder, deposition of calcifications in their soft tissues (muscles, tendons), whereas the patient of 72 years old was also diagnosed with bilateral multifocal eye lesion. Furthermore, and in the latter patient, the patient suffered from multiple spontaneous fractures. On the other hand, the remaining two cases (male patients aged 64 and 69 years old) exhibited no abnormalities in their biochemical analysis of blood.

In our cases, the acquired tomographic signs were characteristic of SCC, namely the chorioretinal complex elevation with an uneven tuberous surface, the presence of a "peak-shaped" contour of the Bruch's membrane, a choroid thinning with increased signal hyperreflectivity, the presence of damage zones in the Bruch's membrane, disorders of the retinal architectonics (thinning due to atrophy of the retinal outer layers in the zones of the Bruch's membrane "peak-shaped" contour and an increase in the retinal thickness because of expansion of the nuclear layers in the Bruch's membrane retraction zones) (Figs. 3, 4). Under the thinned choroid, zones of a local moderately hyporeflective structure were visible (Fig. 5), which is considered as a distinct sign of scleral inner layers lesions [3]. Furthermore, the visualization of the outer border of the choroid was disturbed in the areas of the retinal lesion.

All CO patients' findings (3 patients, 4 eyes) were localized in the central zone of the fundus (juxtapapillary nasally and from below, extending to the foveolar zone, as well as juxtapapillary from the temporal side, without affecting the macular zone).

In two cases, the patients visited the clinic because of a decrease in their visual acuity (a decrease of 0.1 and 0.03, respectively, due to the formation of SNM in the macular zone). The patients were 22 and 35 years of age with binocular and monocular lesions, respectively. The patient with the binocular lesion (Fig. 6), exhibited a MCVA of 1.0 in his fellow eye. In this case, the patient had been noting a gradual decrease in his right eye visual acuity over the past 10 years, because of which he initially received inpatient treatment for central subacute chorioretinitis. Six months prior his visit to the Research Institute of Eye Diseases, a sharp decrease in his vision was noted, and, therefore, a SNM and a single intravitreal administration of anti-VEGF was prescribed.

In another case (Fig. 7), a 35-year-old female patient was diagnosed with a spot on her fundus during typical pregnancy examinations. The patient then noted a decrease in her vision the day after delivery. Six months before her visit to the Research Institute of Eye Diseases, fluorescence angiography was performed in another clinic, where she was diagnosed with peripapillary choroidal neovascularization, for which the patient received three intravitreal injections of the anti-VEGF drug.

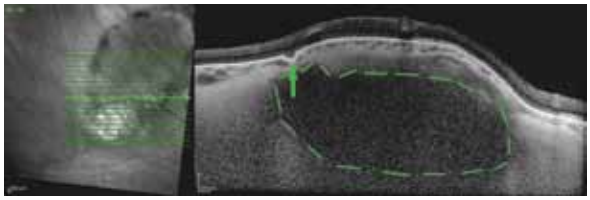

Fig. 5. Optical coherence tomography of the patient Sh. (59 years old). Horizontal scan across sclerochoroidal calcification. Arrow – thinning of the choroid and the zone of Bruch's membrane "entrapment"; dotted line – hyporeflective structure under a thinned choroid

Рис. 5. Оптическая когерентная томография пациентки Ш., 59 лет, горизонтальный срез через зону склерохориоидальной кальцификации. Стрелка — резкое истончение хориоидеи и зона «западения» мембраны Бруха; пунктир — гипорефлективная структура под истончённой хориоидеей

Moreover, a 21-year-old patient was accidentally identified with a small lesion. In this case, MCVA was 1.0 and ophthalmoscopy revealed calcifications along the lower margin of the lesion (Fig. 8).

In all cases, the outer border of the choroid was clearly identified during the OCT examinations. In fact, two tomographic patterns were revealed that had large foci.

1. The presence of an elavated choroidal complex with a mesh structure at the level of the outer layers of the choroid and hyperreflective line separating the tumor from the intact sharply thinned choroid in combination with single local hyperreflective foci at the RPE level (Fig. 9). These zones corresponded to calcified CO [5, 30].

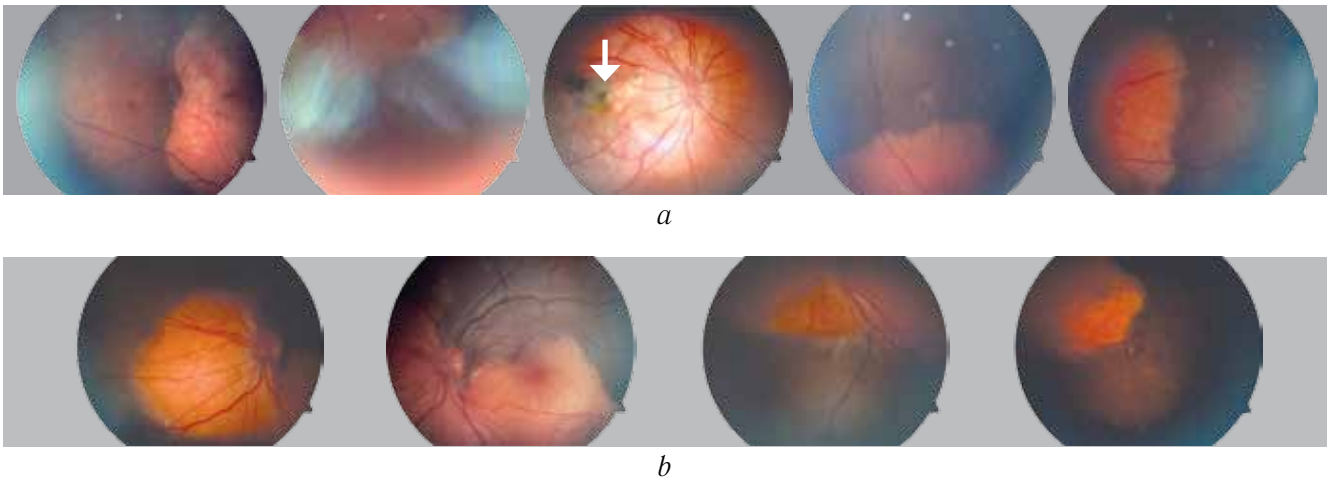

a

b

Fig. 6. Right (*a*) and left (*b*) eye fundus photos of patient G., 22 years old, with bilateral choroidal osteoma. Arrow – choroidal neovascularization

Рис. 6. Фото глазного дна правого (*a*) и левого (*b*) глаза пациента Г., 22 года, с билатеральной остеомой хориоидеи. Стрелка — зона субретинальной неоваскулярной мембраны

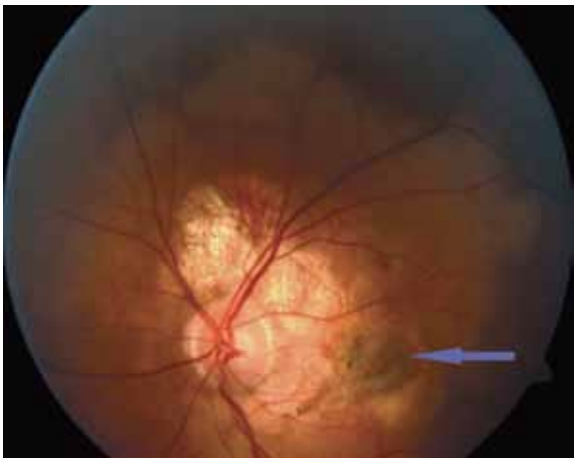

Fig. 7. Fungus photo of patient N., 35 years old. Arrow – choroidal neovascularization

Рис. 7. Фото глазного дна пациентки Н., 35 лет. Стрелка — зона субретинальной неоваскулярной мембраны

Fig. 8. Fundus photo of patient Ch., 21 years old. Arrow – calcification at the inferior edge of the lesion

Рис. 8. Фото глазного дна пациентки Ч., 21 год. Стрелка — кальцинат по нижнему краю очага

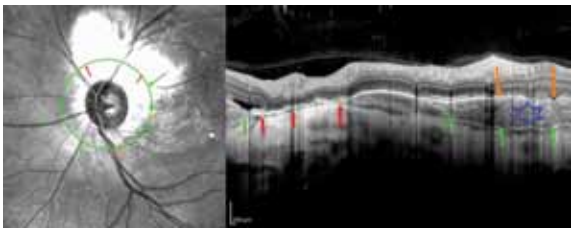

Fig. 9. Optical coherence tomography of the patient N. (35 years old). Circular scan of the peripapillary area. Green arrows – hyperreflective line separating choroidal osteoma from the thinned choroid; orange arrows – zone of impaired Bruch's membrane visualization; asterix – choroid with a "mesh structure"; red arrows – a zone of the dramatic choroidal thinning. Fundus photo – Fig. 7

Рис. 9. Оптическая когерентная томография левого глаза пациентки Н., 35 лет; круговой скан через перипапиллярную зону. Зелёные стрелки — гиперрефлективная линия, отделяющая остеому хориоидеи от истончённой хориоидеи; оранжевые стрелки — зона нарушения визуализации мембраны Бруха; звёздочка — зона хориоидеи с сетчатой структурой; красные стрелки — зона резкого истончения хориоидеи. Фото глазного дна — см. рис. 7

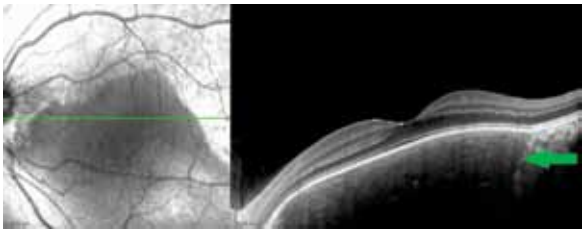

Fig. 10. Optical coherence tomography of the left eye of patient G. (22 years old); horizontal scan across the fovea. Arrow – border between choroidal osteoma and normal choroid. Fundus photo – Fig. 6, *b*

Рис. 10. Оптическая когерентная томография левого глаза пациента Г., 22 года; горизонтальный скан через фовеа. Стрелка — граница остеомы хориоидеи и непоражённой хориоидеи. Фото глазного дна — рис. 6, *b*

2. The presence of a moderately hyperreflective zone of the choroid elevation with a lamellar structure of the choroid complex in the absence of changes in the retina located above, which corresponded to decalcified CO (Fig. 10) [30, 31]. The CO decalcification also resulted to choroid atrophy (Fig. 9) [30].

Furthermore, OCT angiography confirmed the formation of SNM at the border of these patterns (Fig. 11, 12).

The choroidal complex was not elevated in small lesion sizes; however, its structure exhibited changes that were characteristic of calcified CO, with local changes in RPE corresponding to fundus calcification

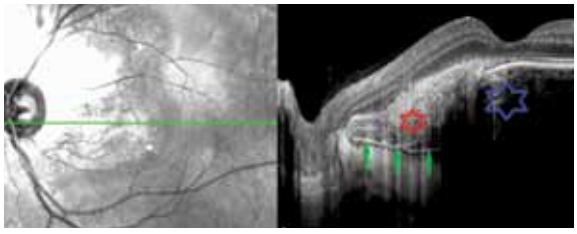

Fig. 11. Optical coherence tomography of the left eye of patient N. (35 years old); horizontal scan across choroidal neovascularization area. Blue asterix – choroid with a "mesh structure", green arrows – hyperreflective line separating choroidal osteoma from the thinned choroid; red asterix – choroid with "lamellar" structure

Рис. 11. Оптическая когерентная томография левого глаза пациентки Н., 35 лет; горизонтальный скан через зону субретинальной неоваскулярной мембраны. Синяя звездочка — зона хориоидеи с сетчатой структурой; зелёные стрелки — гиперрефлективная линия, отделяющая остеому хориоидеи от истончённой хориоидеи; красная звёздочка — зона хориоидеи с пластинчатой структурой

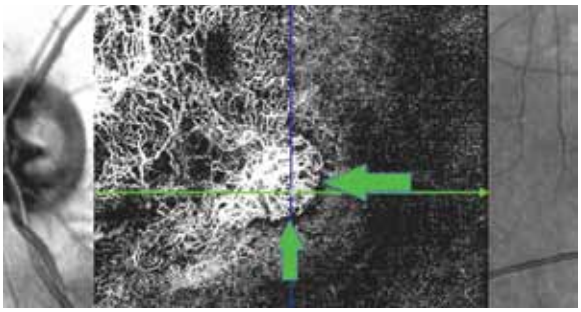

Рис. 12. Оптическая когерентная томография — ангиография того же глаза, сегментация на уровне аваскулярных слоёв сетчатки. Стрелка — зона субретинальной неоваскулярной мембраны

Fig. 12. OCT-angiography of the same eye, segmentation on the level of retinal avascular layers. Arrow – choroidal neovascularization area

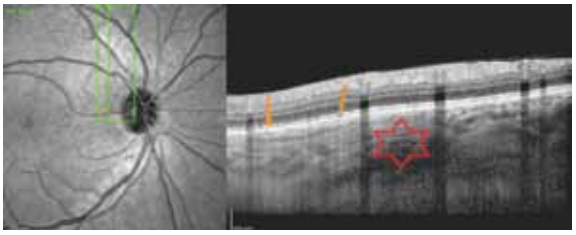

Рис. 13. Оптическая когерентная томография пациентки Ч., 21 год. Вертикальный срез через зону остеомы. Звёздочка — «пластинчатая» структура хориоидеи, стрелка — локальные изменения на уровне ретинального пигментного эпителия. Фото глазного дна — см. рис. 8

Fig. 13. Optical coherence tomography of the patient Ch. (21 years old). Vertical scan across choroidal osteoma. Asterix – choroid with "lamellar" structure, arrow – local changes on the retinal pigment epithelium level. Fundus photo – fig. 8

(Fig. 13). The presence of a calcification zone was also confirmed using ultrasound.

Retinal astrocytoma (2 patients, 2 eyes): The MCVA of the affected eye in both cases was 1.0. In a 76-year-old patient, RA was located in the middle periphery from the temporal side. On the other hand, and for a 32-year old patient, RA was located paramacularly.

In both cases, RAs were revealed accidentally.

RAs were ophthalmoscopically represented by protruding yellowish-white foci with tuberous surfaces (mulberry-shaped) and clear boundaries. A 76-year-old patient presented an extensive area of retinal atrophy around the respective lesion (Fig. 14).

OCT investigations revealed a local elevation of the retinal profile. A thickening of the retinal inner layers was primarily identified at the edges of the lesion and at the nerve fibers layer. On the other hand, large cavities with uneven sharp contours and an intensely hyperreflective wall were noticed in the center of the focus, represented by mulberry-shaped patterns. Multiple hyperreflective inclusions were also found inside the cavities. The choroid thickness in the focal zone did not differ from the adjacent zone, however, it was impossible to evaluate its structure as a result of partial screening and the manifestation of artifacts (Fig. 15), similar to the reverberation effect in US.

The OCT presentation, together with the respective ophthalmoscopic findings, facilitated the diagnosis of RA in these patients.

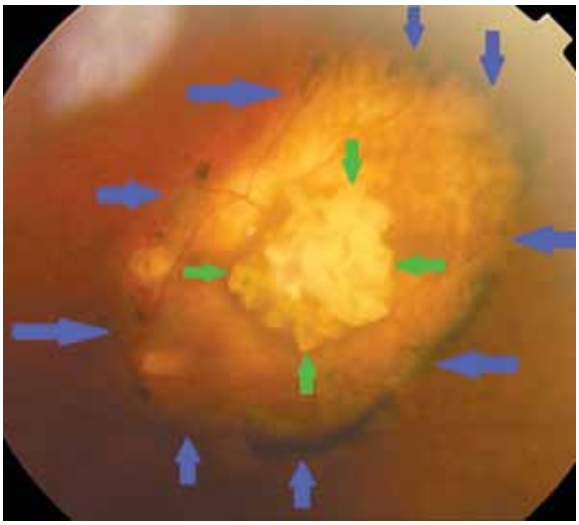

Рис. 14. Фото глазного дна пациентки Д., 76 лет. Синие стрелки — граница зоны атрофии, зелёные стрелки — астроцитома

Fig. 14. Fundus photo of patient D. (76 years old). Blue arrows – zone of retinal atrophy, green arrows – astrocytoma

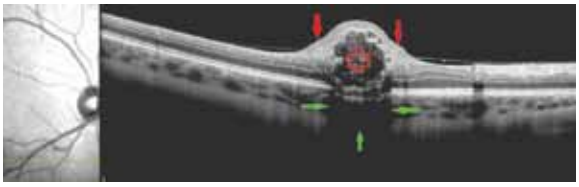

Рис. 15. Оптическая когерентная томография — горизонтальный срез через зону максимальной проминенции астроцитомы сетчатки. Звёздочка — полость в центральной части очага; красные стрелки — утолщение внутренних слоёв сетчатки по краям очага; зелёные стрелки — зона частичного экранирования подлежащих структур

Fig. 15. Optical coherence tomography - horizontal scan across the maximal prominence of retinal astrocytoma. Asterix – a cavity in the center of the focus; red arrows – thickening of the inner layers of the retina along the edges of the focus; green arrows – zone of partial shielding of underlying structures

CONCLUSION

Rare local calcifications of the ocular inner membranes tend to have different etiologies and different levels of damage. In principle, the correct diagnosis can be reached based on the patients' history and a detailed analysis of their ophthalmoscopic images.

However, in complicated cases that tend to exhibit hyperechoic foci with a concurrent acoustic shadow effect in ultrasound, OCT investigations are essential to verify the diagnosis because they allow for a clarification of the level of damage to the ocular inner membranes.

The diagnostic aspect that can distinguish SCC from other conditions involves the localization process along the supero-temporal arcade (ophthalmoscopy data), which according to OCT data, it is the chorioretinal complex elevation with concurrent thinning of the choroid and sections of the "peak-shaped" contour of the Bruch's membrane. From our point of view, the changes detected can confirm previous recommendations made that this process is primarily localized in the sclera [19]. The same can also explain the emergence of retinal changes solely in areas where the choroid was completely absent.

CO is typically located in the central zone of the fundus. Characteristic OCT signs include the expansion of the choroidal complex that exhibits an even profile of the Bruch's membrane surface with the choroid structure disorder (the emergence of its "mesh" or "lamellar" structure). Similar to SCC, retinal damage occurs in the later stages of the process.

Finally, and as opposed to the diseases described above, the pathological process of RA tends to localize in the retinal inner layers. Despite the fact that the choroid remains intact, its visualization is significantly complicated because of pronounced retinal changes (involving a thickening of the retinal inner layers, the presence of large cavities with uneven clear contours and intensely hyperreflective wall, and multiple hyperreflective inclusions), that can, in turn, block the signal stemming from the underlying tissues.

Therefore, a comparison between the biomicro-ophthalmoscopic presentation and the OCT results can establish a precise diagnosis facilitating the development of a treatment plan that will allow efficient patient management.

There is no conflict of interest.

REFERENCES

1. Мякошина Е.Б. Астроцитарная гамартома сетчатки: два клинических случая, визуализация с помощью спектральной оптической когерентной томографии // Российская педиатрическая офтальмология. – 2013. – № 1. – С. 23–27. [Myakoshina EB. Retinal astrocytic harmatoma: two clinical cases, visualization with the help spectral optical coherent tomography. *Russian pediatric ophtalmology.* 2013;(1):23-27. (In Russ.)]
2. Alameddine RM, Mansour AM, Kahtani E. Review of choroidal osteomas. *Middle East Afr J Ophthalmol.* 2014;21(3):244-250. https://doi.org/10.4103/0974-9233.134686.
3. Rao RC, Choudhry N, Gragoudas ES. Enhanced depth imaging spectral-domain optical coherence tomography findings in sclerochoroidal calcification. *Retina.* 2012;32(6):1226-1227. https://doi.org/10.1097/IAE.0b013e3182576e50.
4. Trimble SN, Schatz H. Decalcification of a choroidal osteoma. *Br J Ophthalmol.* 1991;75(1):61-3. https://doi.org/10.1136/bjo.75.1.61.
5. Chen J, Lee L, Gass JD. Choroidal osteoma: evidence of progression and decalcification over 20 years. *Clin Exp Optom.* 2006;89(2):90-94. https://doi.org/10.1111/j.1444-0938.2006.00012.x.
6. Semenova E, Veronese C, Ciardella A, et al. Multimodality imaging of retinal astrocytoma. *Eur J Ophthalmol.* 2015;25(6):559-564. https://doi.org/10.5301/ejo.5000627.
7. Turell ME, Hayden BC, McMahon JT, et al. Uveal schwannoma surgery. *Ophthalmology.* 2009;116(1):163-163. https://doi.org/10.1016/j.ophtha.2008.08.045.
8. Brennan RC, Wilson MW, Kaste S, et al. US and MRI of pediatric ocular masses with histopathological correlation. *Pediatr Radiol.* 2012;42(6):738-749. https://doi.org/10.1007/s00247-012-2374-6.
9. Бровкина А.Ф., и др. Офтальмоонкология: руководство для врачей / под ред. А.Ф. Бровкиной. – М.: Медицина, 2002. – 420 с. [Brovkina AF, et al. Ophthalmooncologiya: rukovodstvo dlya vracey. Ed. by A.F. Brovkina. Moscow: Medicina; 2002. 420 p. (In Russ.)]
10. Williams AT, Font RL, Van Dyk HJ, Riekhof FT. Osseous choristoma of the choroid simulating a choroidal melanoma. Association with a positive 32P test. *Arch Ophthalmol.* 1978;96(10):1874-7187. https://doi.org/10.1001/archopht.1978.03910060378017.
11. Bessho H, Imai H, Azumi A. The histopathological finding of the surgically extracted atypical dome-shaped choroidal osteoma. *Case Rep Ophthalmol Med.* 2017;2017:2874823. https://doi.org/10.1155/2017/2874823.
12. Aksoy Y, Çakir Y, Sevinçli S, et al. Choroidal osteoma in a preterm infant. *Indian J Ophthalmol.* 2018;66(4):583-585. https://doi.org/10.4103/ijo.IJO_914_17.
13. Cennamo G, Romano MR, Iovino C, et al. OCT angiography in choroidal neovascularization secondary to choroidal osteoma. *Acta Ophthalmol.* 2017;95(2): e152-e154. https://doi.org/10.1111/aos.13142.
14. Shields CL, Sun H, Demirci H, Shields JA. Factors predictive of tumor growth, tumor decalcification, choroidal neovascularization,

and visual outcome in 74 eyes with choroidal osteoma. *Arch Ophthalmol.* 2005;123(12):1658-1666. https://doi.org/10.1001/archopht.123.12.1658.
15. MirNaghi M, Nasser S, SeyedehMaryam H1, Ali S. Bilateral multifocal choroidal osteoma with choroidal neovascularization. *Case Rep Ophthalmol Med.* 2015;2015:346415. https://doi.org/10.1155/2015/346415.
16. Aylward GW, Chang TS, Pautler SE, Gass JD. A long-term follow-up of choroidal osteoma. *Arch Ophthalmol.* 1998;116(10):1337-41. https://doi.org/10.1001/archopht.116.10.1337.
17. Sambricio J, Fernández-Reyes M, De-Lucas-Viejo B, et al. A second new choroidal osteoma in the same eye: differences between them with new imaging techniques. *Case Rep Ophthalmol Med.* 2015;2015:684956. https://doi.org/10.1155/2015/684956.
18. Erol MK, Coban DT, Ceran BB, Bulut M. Retinal pigment epithelium tear formation following intravitreal ranibizumab injection in choroidal neovascularization secondary to choroidal osteoma. *Cutan Ocul Toxicol.* 2014;33(3):259-263. https://doi.org/10.3109/15569527.2013.844702.
19. Wong CM, Kawasaki BS. Idiopathic sclerochoroidal calcification. *Optom Vis Sci.* 2014;91(2):e32-37. https://doi.org/10.1097/OPX.0000000000000125.
20. Cooke CA, McAvoy C, Best R. Idiopathic sclerochoroidal calcification. *Br J Ophthalmol.* 2003;87(2):245-246. https://doi.org/10.1136/bjo.87.2.245.
21. Lee H, Kumar P, Deane J. Sclerochoroidal calcification associated with Albright's hereditary osteodystrophy. *BMJ Case Rep.* 2012;2012. pii: bcr0320126022. https://doi.org/10.1136/bcr-03-2012-6022.
22. Gupta R, Hu V, Reynolds T, Harrison R. Sclerochoroidal calcification associated with Gitelman syndrome and calcium pyrophosphate dihydrate deposition. *J Clin Pathol.* 2005;58(12):1334-1335. https://doi.org/10.1136/jcp.2005.027300.
23. Honavar SG, Shields CL, Demirci H, Shields JA. Sclerochoroidal calcification: clinical manifestations and systemic associations. *Arch Ophthalmol.* 2001;119(6):833-840. https://doi.org/10.1001/archopht.119.6.833.
24. Yohannan J, Channa R, Dibernardo CW, et al. Sclerochoroidal calcifications imaged using enhanced depth imaging optical coherence tomography. *Ocul Immunol Inflamm.* 2012;20(3):190-192. https://doi.org/10.3109/09273948.2012.670358.
25. Dedes W, Schmid MK, Becht C. [Sclerochoroidal calcifications with vision-threatening choroidal neovascularisation. (In German)]. *Klin Monbl Augenheilkd.* 2008;225(5):473-475. https://doi.org/10.1055/s-2008-1027276.
26. Pusateri A, Margo CE. Intraocular astrocytoma and its differential diagnosis. *Arch Pathol Lab Med.* 2014;138(9):1250-1254. https://doi.org/10.5858/arpa.2013-0448-RS.
27. Bloom SM, Mahl CF. Photocoagulation for serous detachment of the macula secondary to retinal astrocytoma. *Retina.* 1991;11(4):416-422. https://doi.org/10.1097/00006982-199111040-00009.
28. Shields JA, Shields CL. Glial tumors of the retina. The 2009 king khaled memorial lecture. *Saudi J Ophthalmol.* 2009;23(3-4):197-201. https://doi.org/10.1016/j.sjopt.2009.10.003.
29. Shields CL, Pellegrini M, Ferenczy SR, Shields JA. Enhanced depth imaging optical coherence tomography of intraocular tumors: from placid to seasick to rock and rolling topography – the 2013 francesco orzalesi lecture. *Retina.* 2014;34(8):1495-1512. https://doi.org/10.1097/IAE.0000000000000288.
30. Navajas EV, Costa RA, Calucci D, et al. Multimodal fundus imaging in choroidal osteoma. *Am J Ophthalmol.* 2012;153(5):890-895. https://doi.org/10.1016/j.ajo.2011.10.025.
31. Hayashi Y, Mitamura Y, Egawa M, et al. Swept-source optical coherence tomographic findings of choroidal osteoma. *Case Rep Ophthalmol.* 2014;5(2):195-202. https://doi.org/10.1159/000365184.

Information about the author

Alevtina S. Stoyukhina — PhD, Senior Research Associate of Department of Retina and Optical Nerve Patology. Ophthalmology Department. Research Institute of Eye Diseases, Moscow, Russia. E-mail: a.stoyukhina@ya.ru.

Сведения об авторе

Алевтина Сергеевна Стоюхина — канд. мед. наук, старший научный сотрудник отдела патологии сетчатки и зрительного нерва. ФГБНУ «НИИ глазных болезней», Москва. E-mail: a.stoyukhina@ya.ru.